

Notes on Conformal Invisibility Devices

Ulf Leonhardt

School of Physics and Astronomy, University of St Andrews,
North Haugh, St Andrews KY16 9SS, Scotland

February 9, 2020

Abstract

As a consequence of the wave nature of light, invisibility devices based on isotropic media cannot be perfect. The principal distortions of invisibility are due to reflections and time delays. Reflections can be made exponentially small for devices that are large in comparison with the wavelength of light. Time delays are unavoidable and will result in wave-front dislocations. This paper considers invisibility devices based on optical conformal mapping. The paper shows that the time delays do not depend on the directions of incidence, although the refractive-index profile of any conformal invisibility device is necessarily asymmetric. The distortions of images are thus uniform, which reduces the risk of detection. The paper also shows how the ideas of invisibility devices are connected to the transmutation of force, the stereographic projection and Escheresque tilings of the plane.

PACS 42.15.-i, 02.40.Tt

1 Introduction

The bending of light in dielectric media [1] is the cause of many optical illusions. For example, in a mirage in the desert [2], light rays from the sky are bent above the hot sand where the air is thin and the refractive index is low. In this way the rays minimize their optical paths according to Fermat's Principle [1]. They are creating images of the sky that deceive the observer as illusions of water [2]. Imagine a different situation [3, 4, 5] where a medium guides light around a hole in it such that the rays leave the medium as if nothing were there, see Fig. 1. Any object placed inside would be hidden from sight. The medium would create the ultimate optical illusion: invisibility [3]. Recently, ideas for designing such invisibility devices have been discussed [4, 5]. Ideas for minuscule invisible bodies (smaller than the wavelength of light) are older [6], but first schemes for implementations and interesting twists and methods have been developed recently [7, 8]. Cloaking devices require unusually strong refractive-index profiles, but it is conceivable that they can be built with dielectric metamaterials [7, 8, 9]. Such devices would operate in the microwave region of the electromagnetic spectrum [9] and perhaps also in some frequency windows in the visible range [10].

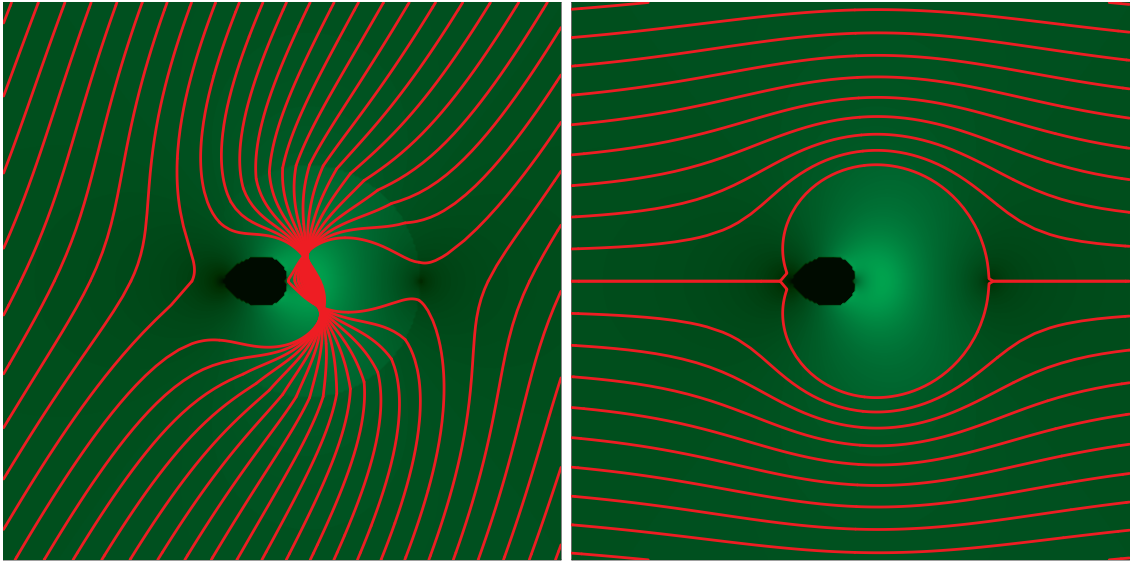


Figure 1: Light propagation in a conformal invisibility device. The light rays are shown in red. The brightness of the green background indicates the refractive-index profile (details given in the Appendix). The device consists of an exterior and an interior layer with a clear boundary. The invisible region is shown in black. Anything could be placed there. The left figure illustrates how light is refracted at the boundary between the two layers and guided around the invisible region where it leaves the device as if nothing were there. In the right figure, light simply flows around the interior layer.

Strictly speaking, ideal invisibility devices based on isotropic media are impossible due to the wave nature of light [11, 12]. Highly anisotropic media, however, may lead, in principle, to the construction of perfect invisibility devices [4]. Expressed in mathematical terms, the inverse scattering problem for linear waves in isotropic media has unique solutions [11]. Therefore, the asymptotic behavior of propagation through empty space, or a uniform medium, is only consistent with the actual propagation through a uniform medium. In theory, nothing can be hidden. In practice, a dielectric invisibility device would perhaps create a slight haze, instead of a perfect image. The principal distortions of invisibility are due to reflections and time delays. Reflections can be made exponentially small for devices that are large in comparison with the wavelength of light [5]. Time delays are unavoidable. They will result in wave-front dislocations at boundaries that lead to image distortions. Wave-front dislocations also pose the risk of detection by sensitive wave-front sensors [13]. In this paper we calculate the time delay caused by the scheme [5] based on optical conformal mapping. We find that the delay is uniform for all directions, although the refractive-index profiles of invisibility devices are necessarily asymmetric [14]. Therefore, the distortions of images composed of various spatial Fourier components are uniform, which reduces the risk of detection.

2 Theory

Our theory is based on geometrical optics [1] and in particular on Fermat's Principle [1] and on Hamilton's analogy [1] between the propagation of light in media and the motion of particles in classical mechanics [15]. Suppose that the refractive index profile $n(\mathbf{r})$ does not vary much over scales comparable with the wavelength of light. In this regime of geometrical optics both polarization components of light ψ for frequencies ω obey the Helmholtz equation [1]

$$\left(\nabla^2 + n^2 \frac{\omega^2}{c^2}\right) \psi = 0 \quad (1)$$

where c denotes the speed of light in vacuum. The Helmholtz equation (1) is equivalent to the stationary Schrödinger equation with potential U and energy E such that [1]

$$U - E = -\frac{n^2}{2}. \quad (2)$$

Therefore we expect that Hamilton's equations for light rays are equivalent to Newton's equations of mechanical particles¹ moving in the potential (2). The frequency ω plays the role of the Hamiltonian and the wavevector \mathbf{k} corresponds to the canonical momentum,

$$\omega = \frac{ck}{n}, \quad k = |\mathbf{k}|. \quad (3)$$

¹Light rays in moving media behave like particles in magnetic fields for low velocities [16, 17, 19] and like particles in gravitational fields [19, 18, 20] in general.

Indeed, we obtain from Hamilton's equations [15] the relations

$$\frac{d\mathbf{r}}{dt} = \frac{\partial\omega}{\partial\mathbf{k}} = \frac{c}{n} \frac{\mathbf{k}}{k} = \frac{c}{n^2\omega} \mathbf{k}, \quad \frac{d\mathbf{k}}{dt} = -\frac{\partial\omega}{\partial\mathbf{r}} = \frac{ck}{2n^3} \nabla n^2 = \frac{\omega}{2n^2} \nabla n^2 \quad (4)$$

that result in the equation of motion for light rays

$$\frac{n^2}{c} \frac{d}{dt} \frac{n^2}{c} \frac{d\mathbf{r}}{dt} = \frac{\nabla n^2}{2}. \quad (5)$$

We can express this equation as Newton's second law

$$\frac{d^2\mathbf{r}}{d\tau^2} = \frac{\nabla n^2}{2} \quad (6)$$

with the effective time increment $d\tau$ measured in spatial units and defined by

$$c dt = n^2 d\tau. \quad (7)$$

Equation (5) also reveals the connection to Fermat's Principle [1]: light in media with refractive index n takes the shortest (or longest) optical path where the optical path length is defined, in Cartesian coordinates, as

$$s = \int n \sqrt{dx^2 + dy^2 + dz^2}. \quad (8)$$

To see this we use the fact that the modulus of the Hamiltonian velocity v equals c/n , a simple consequence of Hamilton's equations (4), and write

$$\frac{n}{v} \frac{d}{dt} \frac{n}{v} \frac{d\mathbf{r}}{dt} = \frac{\nabla n^2}{2}. \quad (9)$$

These are the Euler-Lagrange equations [15] for the effective Lagrangian nv . Hence they minimize or maximize the action (8), which proves Fermat's Principle. The phase of a light ray is given by [1]

$$\phi = \int \mathbf{k} \cdot d\mathbf{r} - \omega t. \quad (10)$$

Along a ray trajectory the phase ϕ is constant. Consequently, the phase delay $\int \mathbf{k} \cdot d\mathbf{r}$ corresponds to ωt . Therefore, the Hamiltonian time t measures the true time delay of light caused by the refractive-index profile, whereas the Newtonian time τ serves as a convenient parameter to characterize the ray trajectories.

Another ingredient of our theory is optical conformal mapping [5]. Consider an effectively two-dimensional case where the medium is uniform in one direction and the light propagates in a plane orthogonal to this axis. It is convenient to use complex numbers $z = x + iy$ for describing the Cartesian coordinates x and y in this plane. In complex notation, the Helmholtz equation (1) assumes the form

$$\left(4 \frac{\partial^2}{\partial z^* \partial z} + n^2 \frac{\omega^2}{c^2} \right) \psi = 0. \quad (11)$$

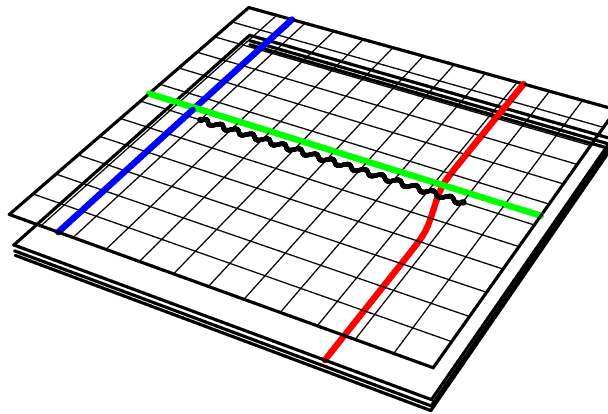


Figure 2: Optical conformal map. A dielectric medium conformally maps physical space described by the points $z = x + iy$ of the complex plane onto a stack of Riemann sheets if the refractive-index profile is $|dw/dz|$ with some analytic function $w(z)$. An invisibility device [5] consists of two layers in real space, as Fig. 1 indicates. On the Riemann surface, the top sheet corresponds to the exterior and the first lower sheet to the interior layer. The figure illustrates the typical fates of light rays in such media. On the Riemann sheets rays propagate along straight lines. The rays shown in blue and green avoid the branch cut and hence the interior of the device. The ray shown in red crosses the cut and passes onto the first lower sheet where it approaches ∞ . However, this ∞ corresponds to a singularity of the refractive index and not to the ∞ of physical space. Rays like this one would be absorbed, unless they are guided back to the exterior sheet.

Suppose that the complex z coordinates are transformed to new coordinates w with an analytic function $w(z)$ that does not depend on the complex conjugate z^* and hence satisfies the Cauchy-Riemann differential equations [21]. Such analytic functions define conformal mappings of the complex plane onto Riemann surfaces [22], see, for example, Fig. 2. Since $\partial/\partial z = (dw/dz) \partial/\partial w$ and $\partial/\partial z^* = (dw^*/dz^*) \partial/\partial w^*$ we obtain in w space the Helmholtz equation (11) with the transformed refractive-index profile n' that is related to n as [5, 23]

$$n = n' \left| \frac{dw}{dz} \right|. \quad (12)$$

On the Riemann surface, light thus propagates according to the refractive index profile n' . The strategy [5] for designing an invisibility device is to take advantage of the sheets of the Riemann surface. Each sheet corresponds to a distinct region in physical space, see, for example, Fig. 3. The branch cuts of the Riemann surface represent the boundaries between the various regions. If one wishes to hide an object, one should hide it on Riemann sheets and prevent light from entering these sheets. To do this, light that has ventured across a branch cut into the interior of the device should be guided back to the exterior. This is done by placing a refractive-index profile on the first interior sheet in which all ray trajectories are closed [5]. The device thus consists of two layers, an outer layer that corresponds to the exterior sheet on the Riemann surface in w space and an inner layer that corresponds to the first interior sheet. For the outer layer we require that the refractive index approaches unity at ∞ , the value for empty space, which implies for the conformal

map

$$w(z) \sim z \quad \text{for } z \rightarrow \infty. \quad (13)$$

At the boundary between the exterior and the first interior sheet light is refracted [1] according to Snell's law², unless it is totally reflected [1, 5]. Since refraction is reversible, the light rays are refracted back to the original direction of incidence when they leave the branch cut to the exterior sheet. Seen on the Riemann surface, light rays perform loops around a branch point that guide them back to the exterior sheet, the outside layer of the device. Seen in physical space, light is guided around the object and leaves the cloaking layers of the device as if nothing were there.

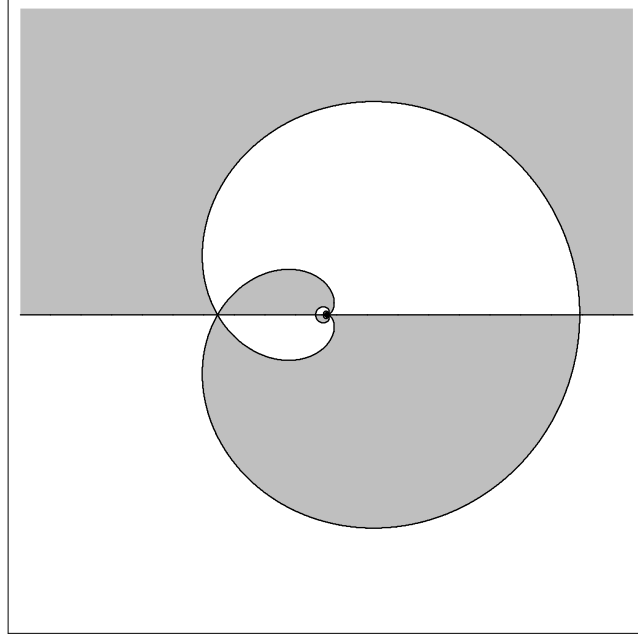


Figure 3: Riemann sheets are tiles. In optical conformal mapping, Riemann sheets represent regions of two-dimensional space, tiles of various forms [21, 22]. The figure illustrates the tiling behind the light propagation of Fig. 1 (details given in the Appendix). The upper imaginary half-plane of each sheet corresponds to a grey tile and the lower half-plane to a white tile. The exterior and the interior sheets of the invisibility device occupy two of such pairs of tiles and the hidden core takes the rest.

3 Time delay

The time delay caused by an invisibility device depends of course on its spatial extension. Imagine that the refractive-index profile $n(\mathbf{r})$ is replaced by $n(\xi\mathbf{r})$ with the constant scale ξ . If $\mathbf{r}(t)$ and $\mathbf{k}(t)$ are solutions of Hamilton's ray equations (4) then $\xi\mathbf{r}$ and \mathbf{k} are solutions, too, if t is replaced by ξt . This proves that the time delay is directly proportional to the spatial extension of the refractive-index profile, as one would expect.

²The law of refraction was discovered by the Arabian scientist Ibn Sahl more than a millennium ago [24].

Since the conformal mapping $w(z)$ is simply a coordinate transformation, the time delay between two points in z space and the delay between the corresponding points in w space are identical. Therefore the part of the refractive-index profile n in physical space that is due to the optical conformal mapping does not influence the time delay at all. Delays are only caused by the index profile in w space that serves to guide light around a branch cut on the first interior sheet. For simplifying the notation, we denote this profile by n (dropping the prime).

Suppose that the transformed refractive-index profile n on the Riemann sheet is radially symmetric with respect to one branch point and designed such that all trajectories of light rays are closed curves around that point. The time delay t_0 of the invisibility device is equal to the time light takes to perform a loop around the branch point. A branch point where ν sheets meet requires ν turns (ν is the winding number). To calculate the delay, we use polar coordinates r and φ centered at the branch point. We obtain from the conservation law of energy [15] for the Newtonian dynamics (6) of light rays

$$\left(\frac{dr}{d\tau}\right)^2 + r^2 \left(\frac{d\varphi}{d\tau}\right)^2 = 2(E - U) = n^2(r). \quad (14)$$

As in the standard theory of motion in central potentials [15] we also use the conservation of the angular momentum,

$$b = r^2 \frac{d\varphi}{d\tau}, \quad (15)$$

written here in terms of the impact parameter b , and obtain from the conservation laws (14) and (15) the relation [23]

$$d\varphi = \frac{b dr}{r \sqrt{n^2 r^2 - b^2}}. \quad (16)$$

To calculate the time delay, we express the Hamiltonian time increment (7) in terms of $d\varphi$, utilizing the conservation of the angular momentum (15). Then we use the relation (16) to write the time delay as an integral over the radial range of the trajectory. The range of r is bounded by the radial turning points r_{\pm} where $dr/d\varphi$ vanishes, which implies

$$n^2(r_{\pm})r_{\pm}^2 = b^2. \quad (17)$$

One trajectory between r_- and r_+ corresponds to half a turn around the branch point. Consequently,

$$\frac{ct_0}{2\nu} = \int_{r_-}^{r_+} \frac{n^2 r dr}{\sqrt{n^2 r^2 - b^2}} = \int_{r_-}^{r_+} \sqrt{n^2 r^2 - b^2} \frac{dr}{r} + b\varphi. \quad (18)$$

In general, the time delay depends on the impact parameter. However, for closed loops, t_0 turns out to be independent of b . To see this, we differentiate the time delay (18) with respect to the impact parameter b and obtain from Eqs. (16) and (17)

$$c \frac{dt_0}{db} = 2\nu b \frac{d\varphi}{db} = 0, \quad (19)$$

because, when all loops around the branch point are closed, φ reaches π regardless of the value of b . Consequently, the time delay does not depend on the direction at which light has entered the branch cut to the first interior sheet, *i.e.* the interior layer of the device. The invisibility device causes a uniform time delay.

4 Examples

Reference [5] mentions two examples of refractive-index profiles on the interior sheet that can be used to circumnavigate the branch point such that all loops are closed, the harmonic-oscillator profile

$$n_1 = \sqrt{1 - r^2/r_1^2} \quad (20)$$

that is related to a Luneburg lens [23, 25] and the Kepler profile [23, 25]

$$n_2 = \sqrt{r/r_2 - 1} \quad (21)$$

that is related to an Eaton lens [25]. Here r_1 and r_2 are constants that describe the ranges of the refractive-index profiles. Seen on the Riemann surface, light cannot penetrate the outside of circles of radii r_1 and r_2 , respectively, because here the refractive index would be purely imaginary. The optical conformal mapping turns areas on the first interior sheet inside out [21, 22]. Therefore, the exterior of these circles corresponds to the invisible interior of the device.

The harmonic-oscillator and the Kepler potential are the only spherically symmetric potentials U where the trajectories for all bound-state energies E are closed [15]. However, what matters in the propagation of light rays is the difference (2) between U and E . Therefore it is sufficient when for a specific value of E the trajectories for all angular-momenta b are closed. A known example where this is the case is Maxwell's fish eye [1, 23, 25, 26] with the refractive-index profile

$$n_3 = \frac{n_0}{1 + (r/r_3)^2} . \quad (22)$$

The constant radius r_3 characterizes the scale of the index profile and n_0 is a parameter that defines the refractive index at the branch point. If Maxwell's fish eye is employed to guide light back to the exterior Riemann sheet, the entire interior sheet is reached by the incident light. However, when the Riemann surface contains more sheets than the exterior and the first interior sheet, all the remaining sheets are hidden. Anything placed there is invisible.

The Newtonian equation of motion for rays generated by the harmonic-oscillator profile (20) describes Hooke's law of a force proportional to the distance, whereas the Kepler profile (21) generates Newton's inverse-square law. In both cases, the trajectories form ellipses for all bound states, a fact that Newton found exceptionally remarkable [27, 28]. However, Hooke's law and Newton's law can be transformed into each other³ by a transmutation of force according to the Arnol'd-Kasner theorem [29, 30, 31].

³Ironically, despite Newton and Hooke reportedly having been bitter rivals, their most celebrated force laws are essential identical [29, 30, 31].

4.1 Hooke's force

In the case of the harmonic-oscillator profile (20) the ray trajectories are very simple [15]: they form a set of ellipses centered at the origin (the branch point), see Fig. 4. To calculate the time spent along a given ellipse we use Cartesian coordinates x

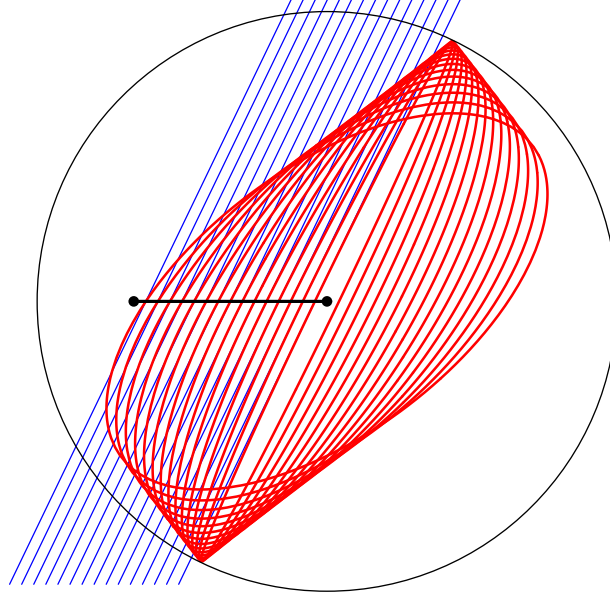


Figure 4: Light guiding using Hooke's law (a Luneburg lens). The device guides light that has entered its interior layer back to the exterior, represented here using two Riemann sheets that correspond to the two layers, seen from above. At the branch cut, the thick line between the two points in the figure, the branch points, light passes from the exterior to the interior sheet. Here light is refracted according to Snell's law, see Eq. (A8) of the Appendix. On the lower sheet, the refractive-index profile (20) guides the rays to the exterior sheet in elliptic orbits with one branch point in the centre. Finally, the rays are refracted back to their original directions and leave on the exterior sheet as if nothing had happened. The circle in the figure indicates the maximal elongations of the ellipses. This circle limits the region in the interior of the device that light does not enter. The outside of the circle corresponds to the inside of the device. Anything beyond this circle is invisible.

and y rotated such that they match the axes of this ellipse. We describe the ellipse as

$$x = a \cos \xi, \quad y = b \sin \xi, \quad \xi = \tau/r_1 \quad (23)$$

with the constants a and b being the axis lengths. One easily verifies that the trajectory (23) solves the Newtonian equation of motion (6). The ray trajectory corresponds to the Newtonian energy $1/2$, which implies

$$2E = \left(\frac{dx}{d\tau}\right)^2 + \left(\frac{dy}{d\tau}\right)^2 + \frac{x^2 + y^2}{r_1^2} = \frac{a^2 + b^2}{r_1^2} = 1. \quad (24)$$

Consequently, we obtain for the time delay

$$ct_0 = \oint n^2 d\tau = \nu r_1 \int_0^{2\pi} \left(1 - \frac{a^2}{r_1^2} \cos^2 \xi - \frac{b^2}{r_1^2} \sin^2 \xi \right) d\xi = \nu \pi r_1. \quad (25)$$

In agreement with our general results, the time delay caused by the harmonic-oscillator profile depends on the spatial extension r_1 and is otherwise uniform.

4.2 Newton's force

In order to calculate the time delay caused by the Kepler profile (21), see Fig. 5, we use the transmutation of force [29, 30, 31] to the harmonic-oscillator profile, *i.e.* the transformation of Newton's law into Hooke's law that is also based on conformal mapping [22]. Consider trajectories in the complex plane, say the z plane, although

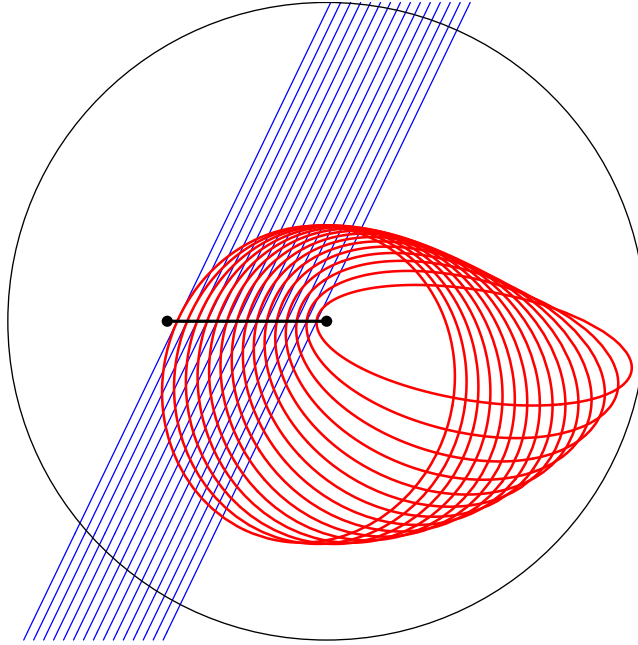


Figure 5: Light guiding using Newton's law (an Eaton lens) similar to Fig. 4. Light is guided in elliptic orbits with one branch point in the focal point, instead of the centre, as in Hooke's case.

in our case this plane is one of the Riemann sheets generated by the optical conformal mapping in the first place. Suppose that the trajectories are conformally mapped by the analytic function $w(z)$. We obtain from Eqs. (2) and (12) the relations

$$U - E = -\frac{n^2}{2} = -\frac{n'^2}{2} \left| \frac{dw}{dz} \right|^2 = (U' - E') \left| \frac{dw}{dz} \right|^2. \quad (26)$$

Consequently, if the potential U can be written as the modulus square of an analytic function, the potential U' is proportional to the modulus square of the inverse of

this function expressed in terms of the new coordinates,

$$U(z) = -E' \left| \frac{dw(z)}{dz} \right|^2, \quad U'(w) = -E \left| \frac{dz(w)}{dw} \right|^2. \quad (27)$$

The trajectories are mapped onto each other by the transformation $w(z)$. The potentials U and U' are thus related to each other, generating dual forces [29]. Consider

$$w = \frac{z^2}{2r_1}, \quad E' = -\frac{1}{2}. \quad (28)$$

The map $w(z)$ corresponds to the Hooke potential (2) of the harmonic-oscillator profile (20) with energy $E = 1/2$ and, in turn, $w(z)$ generates the Kepler profile (21) that corresponds to Newton's inverse square law with the parameter

$$r_2 = \frac{r_1}{2}. \quad (29)$$

Since conformal mapping does not influence the time delay in light propagation, the delay generated by the Kepler profile (21) corresponds to that of the harmonic-oscillator profile (20), apart from one subtlety: already a half-ellipse of the harmonic-oscillator is mapped onto a complete Kepler ellipse, because of the square map (28). Consequently, the time delay is

$$ct_0 = \frac{\nu}{2} \pi r_1 = \nu \pi r_2, \quad (30)$$

in complete analogy to the result (25) for the harmonic-oscillator profile. The time delays are thus identical for identical ranges r_1 and r_2 of the refractive-index profiles.

4.3 Maxwell's fish eye

Maxwell's fish eye turns out to represent another classic conformal mapping [23], the stereographic projection discovered by Ptolemy and applied in the Mercator map projection⁴. Figure 6 shows how the points on the surface of a sphere (X, Y, Z) are mapped onto a plane, say the z plane, according to the formulas [21, 31]

$$z = x + iy = \frac{X + iY}{1 - Z}, \quad X^2 + Y^2 + Z^2 = r_3^2 \quad (31)$$

with the inverse

$$X + iY = \frac{2z}{1 + |r/r_3|^2}, \quad Z = r_3 \frac{|r/r_3|^2 - 1}{|r/r_3|^2 + 1}, \quad r^2 = x^2 + y^2. \quad (32)$$

We find that the square of the optical-length element (8) for Maxwell's fish eye (22) is

$$ds^2 = n_0^2 \frac{dx^2 + dy^2}{(1 + |r/r_3|^2)^2} = \frac{n_0^2 r_3^2}{4} (dX^2 + dY^2 + dZ^2). \quad (33)$$

⁴The Mercator map projection is the logarithm of the stereographic projection [31].

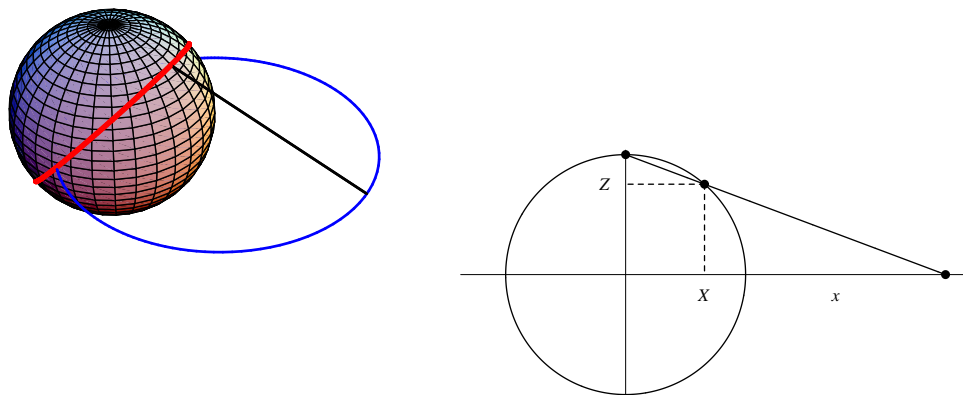


Figure 6: Stereographic projection, mapping the (x, y) plane onto the (X, Y, Z) surface of a sphere. A line drawn from the North Pole of the sphere to (x, y) cuts the surface of the sphere at (X, Y, Z) . Circles on the plane are mapped into circles on the sphere and vice versa [31].

Consequently, the light rays of the fish eye are mapped into rays on the surface of a sphere with radius r_3 and uniform refractive index $n_0/2$. According to Fermat's Principle [1], the rays are geodesics, lines of extremal optical path length, see Fig. 7. On a uniform sphere, the geodesics are the great circles. Since they are closed curves on the sphere, the light rays are closed on the plane as well, as we required. Furthermore, the stereographic projection maps circles onto circles [31] and so the light rays in Maxwell's fish eye (22) form circles in the plane [1, 23, 25].

The calculation of the time delay of light circling in Maxwell's fish eye is elementary now, because t_0 does not depend on conformal transformations and in particular on the stereographic projection (32); t_0 simply is the time delay of light during ν loops on the surface of a sphere with radius r_3 and refractive index $n_0/2$, which gives

$$ct_0 = \nu \frac{n_0}{2} 2\pi r_3 = \nu \pi r_3 n_0. \quad (34)$$

In agreement with our general results, the time delay is proportional to the length scale of the refractive-index profile and is uniform for all directions of incidence.

5 Conclusions

In isotropic media, no illusion is perfect due to the wave nature of light [11]. Consequently, conformal invisibility devices [5] cannot be perfect; they cause reflections and time delays. However, the reflectivity can be made exponentially small for macroscopic devices and the time delay is uniform for all directions. This is important, because images consist of light propagating in a range of directions, having a range of spatial Fourier components. The time delay occurs when the light reaches

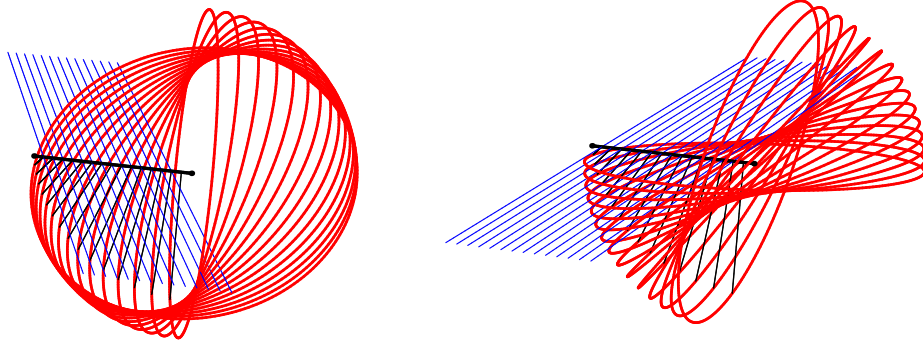


Figure 7: Light guiding using Maxwell's fish eye. The interior layer of the invisibility device is represented by a sphere of radius r_3 . At the boundary, the branch cut, the light drops onto the sphere where it propagates in great circles. After jumping up to the exterior sheet the light rays leave the device. This behavior is generated by the refractive-index profile of Maxwell's fish eye (22) that represents the stereographic projection illustrated in Fig. 6 as an optical conformal mapping. The pictures illustrates light propagation for angles of incidence of $\pm\pi/7$.

the interior layer of the device. It will cause wavefront dislocations at the two sides. The diffraction of light will slightly blur the image, but the haze caused is uniform.

Acknowledgments

Many people have contributed to my obsession with invisibility. I am particularly grateful to Greg Gbur for our discussions in Kiev on the impossibility of invisibility and for his exquisite review article, to Mark Dennis for introducing me to the transmutation of force and to Awatif Hindi for her advice on elliptic modular functions. My work has been supported by the Leverhulme Trust and the Engineering and Physical Sciences Research Council.

6 Appendix

The pictures of this paper are based on a conformal map using elliptic modular functions [32]. These functions are connected to many branches of mathematics, including the proof of Fermat's Last Theorem [33]. We adopt the notation of the Bateman Manuscript Project on Higher Transcendental Functions [32] (not Neharis notation⁵). We use the modular function J known as the Klein invariant, illustrated

⁵In Neharis book [22] $\lambda(z)$ is denoted as $J(z)$.

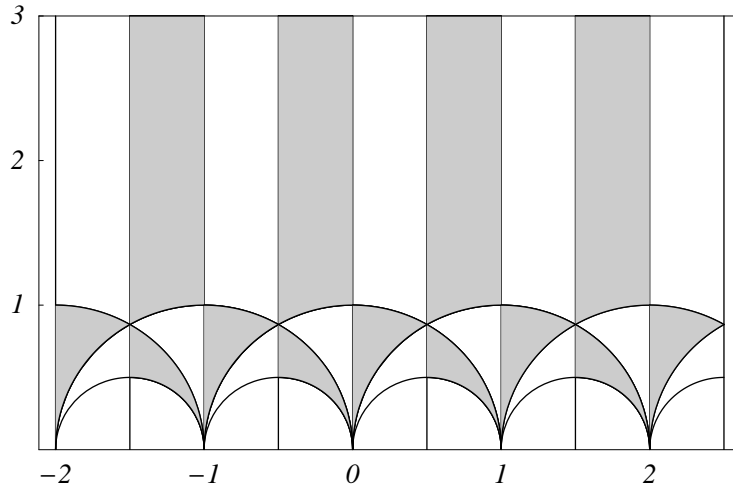


Figure 8: The Klein invariant $J(z)$ tiles the upper half z plane with an infinite sequence of circular arches. The arches continue near the real axis in an infinitely intricate structure (not shown here). Identifying all horizontal strips of length 1 and deforming the outer arch to a circle leads to Fig. 3 that illustrates the tiling of the optical conformal map (A3).

in Fig. 8, and expressed here in terms of the modular function λ as

$$J(z) = \frac{4}{27} \frac{(1 - \lambda + \lambda^2)^3}{\lambda^2(1 - \lambda)^2}, \quad \lambda = 16q \left(\frac{\sum_{m=0}^{\infty} q^{m(m+1)}}{1 + 2 \sum_{m=1}^{\infty} q^{m^2}} \right)^4 \quad (\text{A1})$$

with

$$q = e^{i\pi z}, \quad |q| < 1, \quad (\text{A2})$$

see Eqs. (36-38) of Ref. [32]. Note that the expression for λ is rapidly converging and therefore well suited for numerical computations. Consider the map

$$w = 4r_0 J \left(-\frac{\ln(432z/r_0)}{2\pi i} \right) - \frac{31r_0}{18} = \frac{16r_0}{27} \frac{(1 - \lambda + \lambda^2)^3}{\lambda^2(1 - \lambda)^2} - \frac{31r_0}{18} \quad (\text{A3})$$

with

$$q = \frac{1}{\sqrt{432z/r_0}}. \quad (\text{A4})$$

The constant r_0 characterizes the spatial scale of the optical conformal mapping. Far away from the device light should propagate through empty space, which implies that $w \sim z$ for $z \rightarrow \infty$. The map (A3) is chosen such that this is the case. Indeed, we obtain from the representation (A1) the first terms of the Laurent expansion

$$J \sim \frac{1}{1728q^2} + \frac{31}{72} + \frac{1823}{16} q^2 \quad \text{for } q \rightarrow 0, \quad (\text{A5})$$

which implies, according to Eqs. (A3) and (A4),

$$w \sim z + \frac{1823}{1728} \frac{r_0^2}{z} \quad \text{for } z \rightarrow \infty. \quad (\text{A6})$$

In the exterior of the device, the map (A3) approaches the simple example considered in Ref. [5], whereas in the interior the map (A3) represents the infinitely more complicated Riemann surface illustrated in Figs. 3 and 8. The Riemann surface contains three branch points [22, 32], $w_1 = (41/18)r_0$, $w_2 = -(31/18)r_0$ and $w_\infty = \infty$ with winding numbers 1, 2 and ∞ , apart from the exterior sheet with only w_1 and w_2 [22, 32].

In order to calculate the ray trajectories, we consider the ray dynamics in w space and then transform w to the physical trajectories in z space. We describe both the ray trajectories w and the wavevectors k by complex numbers. In the exterior sheet light propagates along straight lines. Given a point w on the exterior sheet, we numerically solve Eq. (A3) for z using the inversion $z(w)$ of the asymptotic map (A6) as the starting value,

$$z \sim \frac{1}{72} \left(36w + \sqrt{3(432w^2 - 1823)} \right) \quad (\text{A7})$$

for $\text{Im}w \geq 0$ and we use $z^*(w^*)$ otherwise. At the branch cut between the exterior and the first interior sheet light is refracted according to Snell's law [1, 24]. Since the modulus of k equals $n(\omega/c)$, we obtain for a light ray incident at the angle φ Snell's law in complex notation as

$$k = \frac{\omega}{c} \left(\sin \varphi - i\sqrt{n^2 - \sin^2 \varphi} \right). \quad (\text{A8})$$

On the first interior sheet, we solve Hamilton's equations for a radially symmetric index profile around the branch point w_1 ,

$$\frac{dw}{dl} = \frac{k}{n(|w - w_1|)|k|}, \quad \frac{dk}{dl} = \frac{n_r(|w - w_1|)|k|}{n^2(|w - w_1|)} \frac{w}{|w|}, \quad n_r(r) = \frac{dn(r)}{dr} \quad (\text{A9})$$

for the propagation distance $l = ct$ and Maxwell's fish eye (22) with $n = n_3$, $r_3 = 4r_0$ and $n_0 = 2$. The parameters are designed such that the refractive index on the Riemann structure reaches 1 at the other branch point w_2 and exceeds 1 along the branch cut. In this way, total reflection is excluded for the lowest possible value of n_0 . To calculate $z(w)$ on the first interior sheet we utilize the modular symmetry of the Klein invariant [32],

$$J(z') = J(z) \quad \text{for} \quad z' = -z^{-1}, \quad (\text{A10})$$

which leads to

$$z' = \frac{r_0}{432} \exp \left(\frac{4\pi^2}{\ln(432z/r_0)} \right) \quad (\text{A11})$$

for the position z' that shares the same numerical value of w as z , but corresponds to the first interior sheet. We follow the same procedure as for the exterior layer of the device to calculate z and then transform it into z' to continue the trajectory in the interior layer.

References

- [1] M. Born and E. Wolf, *Principles of Optics* (Cambridge University Press, Cambridge, 1999).
- [2] R. P. Feynman, R. B. Leighton, and M. Sands, *The Feynman lectures on physics. Mainly mechanics, radiation and heat*. Chapter 26 (Addison Wesley, Reading, Mass., 1983).
- [3] G. Gbur, Prog. Opt. **45**, 273 (2003).
- [4] J. B. Pendry, D. Schurig, and D. R. Smith, Science (in press).
- [5] U. Leonhardt, Science (in press); arXiv:physics/0602092.
- [6] M. Kerker, J. Opt. Soc. Am. **65**, 376 (1975).
- [7] A. Alu and N. Engheta, Phys. Rev. E **72**, 016623 (2005).
- [8] G. W. Milton and N.-A. P. Nicorovici, Proc. Roy. Soc. London A **462**, 1364 (2006).
- [9] D. R. Smith, J. B. Pendry, and M. C. K. Wiltshire, Science **305**, 788 (2004).
- [10] A. N. Grigorenko, A. K. Geim, H. F. Gleeson, Y. Zhang, A. A. Firsov, I. Y. Khrushchev, and J. Petrovic, Nature **438**, 335 (2005).
- [11] A. I. Nachman, Ann. Math. **128**, 531 (1988).
- [12] E. Wolf and T. Habashy, J. Mod. Opt. **40**, 785 (1993).
- [13] R. K. Tyson, *Principles of adaptive optics* (Academic, Boston, 1991).
- [14] A. Hendi, J. Henn, and U. Leonhardt, arXiv:cond-mat/0605637.
- [15] L. D. Landau and E. M. Lifshitz, *Mechanics* (Pergamon, Oxford, 1976).
- [16] J. H. Hannay, Cambridge University Hamilton prize essay 1976 (unpublished).
- [17] R. J. Cook, H. Fearn, and P. W. Milonni, Am J. Phys. **63**, 705 (1995).
- [18] W. Gordon, Ann. Phys. (Leipzig) **72**, 421 (1923).
- [19] U. Leonhardt and P. Piwnicki, Phys. Rev. A **60**, 4301 (1999).
- [20] U. Leonhardt, Phys. Rev. A **62**, 012111 (2000).
- [21] M. J. Ablowitz and A. S. Fokas, *Complex Variables* (Cambridge University Press, Cambridge, 1997).
- [22] Z. Nehari, *Conformal Mapping* (McGraw-Hill, New York, 1952).

- [23] R. K. Luneburg, *Mathematical Theory of Optics* (University of California Press, Berkeley and Los Angeles, 1964).
- [24] R. Rashed, *Isis* **81**, 464 (1990).
- [25] M. Kerker, *The Scattering of Light* (Academic Press, New York, 1969).
- [26] J. C. Maxwell, *Cambridge and Dublin Math. J.* **8**, 188 (1854).
- [27] I. Newton, *Philosophiae Naturalis Principia Mathematica* (Cambridge University Press, Cambridge, 1687).
- [28] S. Chandrasekhar, *Newton's Principia for the Common Reader* (Clarendon Press, Oxford, 1995).
- [29] V. I. Arnol'd, *Huygens & Barrow, Newton & Hooke* (Birkhäuser Verlag, Basel, 1990).
- [30] T. Needham, *Amer. Math. Monthly* **100**, 119 (1993).
- [31] T. Needham, *Visual Complex Analysis* (Clarendon Press, Oxford, 2002).
- [32] A. Erdélyi, W. Magnus, F. Oberhettinger, and F. G. Tricomi, *Higher Transcendental Functions*, Vol. III, Sec. 14.6 (McGraw-Hill, New York, 1981).
- [33] A. Wiles, *Ann. Math.* **141**, 443 (1995).